DOI: https://doi.org/10.24425/amm.2024.147805

UIJUN-KO[1], BYUNGJUN-HAN[1], KYOUNG-TAE PARK[2*],
MARZIEH-EBRAHIMIAN[1], JH-KIM[1*]

MICROSTRUCTURE EVOLUTION THROUGH CRYOGENIC ROLLING OF ULTRA-HIGH PURITY TITANIUM PRODUCED BY ELECTRON BEAM MELTING

In this study, crystal grain refinement of pure titanium manufactured by electron beam melting through cryogenic rolling was performed. The effect of rolling in a cryogenic atmosphere on average grain size was investigated. Cryogenic atmosphere rolling was confirmed to be smaller than normal temperature rolling. Electron back scatter diffraction (EBSD) confirmed the presence of oriented crystal grains in the material. The deformation, temperature, and stress generated during rolling were calculated using 3D simulation. Finite element analysis (FEM) modeling was used to analyze the trend of average grain size change during the heat treatment of the rolled samples.

Keywords: Pure titanium; Cryogenic roll; Simulation modeling

1. Introduction

The demand for ultrahigh-purity titanium (UP-Ti) for use as sputtering targets is increasing [1-4]. Recently, the electron beam melting process (EBM) has enabled the manufacturing of UP-Ti with a purity level of 4N5 (99.995%) or higher [5-12]. The EBM process utilizes an electron beam to melt the metal powder and shape it into a desired form. EBM occurs under high-vacuum conditions, allowing impurities to volatilize, thus producing a high-purity final product. However, high-purity ingots manufactured using the EBM process have coarse grain sizes and relatively irregular textures. Previous studies have demonstrated that targets with smaller grain sizes exhibit higher deposition rates compared to those with larger grain sizes [13-15]. This is because grain boundaries are more vulnerable to attack during sputtering. The higher the grain boundary area, the faster the film deposition. In addition, the crystallographic orientation must be aligned along the (0001) direction to improve the uniformity of the sputtered film [16-18].

In the case of UP-Ti manufactured by EBM, the vapor pressure differences between titanium and other elements, such as oxygen and iron, leads to substantial evaporation of these impurities, resulting in higher purity. However, the high purity of UP-Ti also leads to low lattice friction and weak grain boundary pinning forces, which in turn contribute to a remarkably high grain growth rate [19-21]. For its application as a sputtering target, UP-Ti needs to possess a fine grain size below 30 μm and a strong (0001) texture orientation along the ND (normal direction). Cryogenic rolling below –70°C is a useful process for obtaining fine grain structures and controlled texture characteristics that are difficult to achieve using conventional rolling and forging processes [22-24].

In the present study, crystal grain refinement of UP-Ti ingots produced by EBM through cryogenic rolling was performed. Rolling was carried out at room temperature and –75°C. After rolling, heat treatment was performed at 800°C for 5, 15, and 30 minutes to investigate the changing grain size.

2. Experimental details

UP-Ti ingots produced using the EBM process (Production Technology Research Institute) were used in this study. A beam current of 500 mA was applied for 1 hour to produce a 900 g ingot. Owing to the high-vacuum electron beam melting, the oxygen content of the UP-Ti ingots was measured as 1218 ppm, far below that of commercially pure Ti (1800 ppm for CP-Ti grade 1). The UP-Ti ingots were rolled at room

[1] HANBAT NATIONAL UNIVERSITY, DEPARTMENT OF MATERIALS SCIENCE AND ENGINEERING, YUSEONG-GU, DAEJEON 34158, REPUBLIC OF KOREA
[2] RAREMETAL R&D GROUP, KOREA INSTITUTE OF INDUSTRIAL TECHNOLOGY, 12, GAETBEOL-RO, YEONSU-GU, INCHEON, 21999, REPUBLIC OF KOREA

* Corresponding authors: ktpark@kitech.re.kr; kimjh000@gmail.com

temperature (25°C) and cryogenic temperature (–75°C). Each sample was designated as an room temperature (RT) or cryogenic temperature (CT sample. The initial ingot size for rolling was 50 mm × 20 mm × 17 mm. After 18 rolling passes, the ingot height decreased to 5.6 mm. Ethanol was cooled to –75°C to create a cryogenic atmosphere, and the rolled CT samples were cooled for a sufficient amount of time before each pass. After rolling, the specimens were heat-treated at 800°C for 5, 15, and 30 min.

The samples were rolled and heat treated under each condition and etched using an electropolishing machine (electropol-5, Struers). Etching was performed using 95% methanol and 5% perchloric acid etchant for 10 seconds at –20°C, and 30 V was applied. The microstructures of the etched samples were examined using an optical microscope (OLYMPUS Co. GX41 model) and electron backscattered diffraction (TSL Hikari XP) [25]. The average grain size was determined by analyzing the optical microscope data using ImageJ software [26,27].

Using the finite element method with the DEFORM-3D code [28,29], the distributions of temperature, applied stress, and strain were simulated. The reliability of the simulation results was confirmed by comparing the height measured after the pass with that calculated during the pass.

3. Results and discussion

Fig. 1 shows the optical micrographs of UP-Ti before and after rolling. Fig. 1a shows that the as-received microstructure produced by the EBM process is composed of a lamellar phase structure. The lamellar thickness was approximately 20-100 mm. Fig. 1b shows the long-stretched coarse-phase structure of the RT sample after room-temperature rolling. Fig. 1c shows the microstructures of the CT samples after rolling at cryogenic temperatures. After cryogenic rolling, the microstructure of the specimen exhibited a thinner-phase structure compared to that of the specimen rolled at room temperature. This suggests that cryogenic rolling transferred more stress compared to normal temperature rolling, attributed to the generation of slip and the increased occurrence of twins during cryogenic rolling, leading to higher internal stress and reduced grain size during recrystallization. Deformation twinning has been reported to create high-angle twin boundaries within the grain matrix, causing grain fragmentation and leading to grain refinement [23].

The effects of cryogenic rolling are illustrated in Fig. 2. The grain size of the rolled sample increased significantly with heat treatment at 800°C. Under the same heat-treatment conditions, the average grain size of the CT sample was considerably smaller than that of the RT sample. Fig. 2(a-f) confirms this finding. Fig. 2(g) shows the average grain size plot as a function of annealing time at 800°C. Notably, the grain growth rate of UP-Ti is much faster than that of conventional CP-Ti. This is because the amount of impurities that can interfere with atomic movement or diffusion is very low in UP-Ti.

Fig. 3 shows the EBSD data of the sample subjected to heat treatment for 5 min after rolling. Twin structures disappeared for both the RT and CT samples because of recrystallization. Moreover, both RT samples had a strong basal texture. However, compared to the CT, the basal texture of the RT deviated more from the ND direction. For example, the (0001) pole figure of the RT sample consists primarily of a split basal texture towards

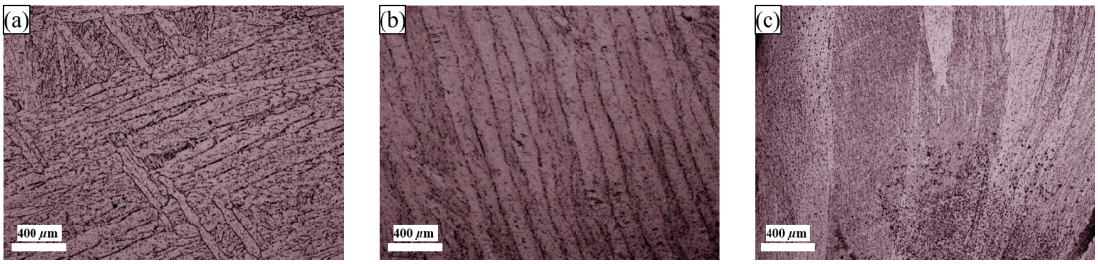

Fig. 1. Optical images of (a) as-received UP-Ti after EBM, (b) microstructure after room temperature rolling, and (c) cryogenic rolling, respectively

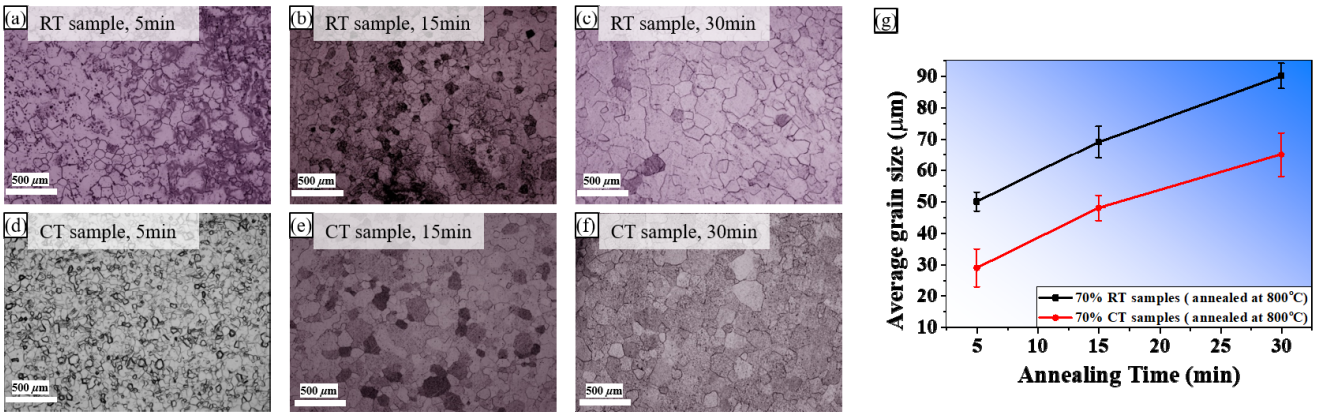

Fig. 2. Optical images of microstructure after heat treatment for (a, d) 5 min, (b, e) 15 min, (c, f) 30 min. (a, b, c) for RT samples, (d, e, f) for CT samples. (g) Average grain size of the microstructure of UP-Ti ingot as a function of annealing time

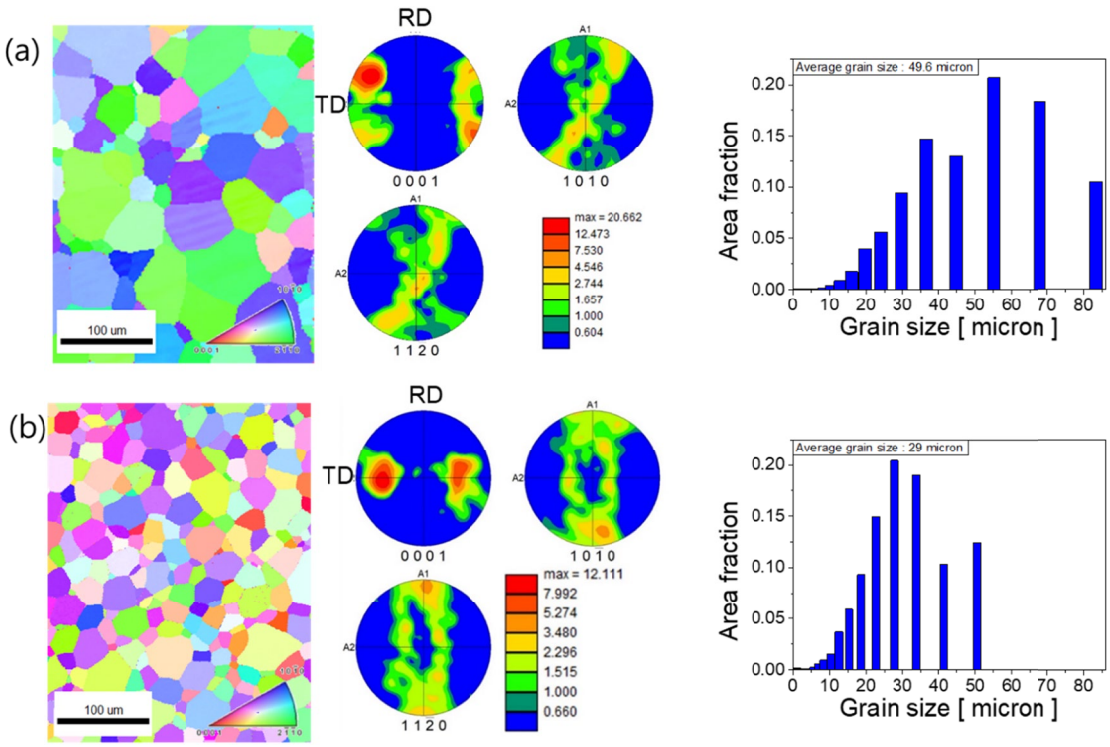

Fig. 3. EBSD data of (a) RT and (b) CT samples after heat treatment

the TD and RD at an angle of ~80°, while that of the CT sample shows a split basal texture towards the TD at an angle of ~45°. The average grain size of the RT sample was ~50 micrometers, while the average grain size of the CT samples subjected to the same heat treatment was ~29 micrometers, in line with Fig. 2. In addition, the standard deviation of the grain size distribution was much smaller at CT than at RT. These results indicate that the microstructure of UP-Ti, suitable for sputtering target materials, is better controlled through cryo-rolling. Therefore, a uniform and fast deposition can be achieved by controlling the crystal structure of pure Ti via cryogenic rolling.

The stress, strain, and temperature during cryogenic rolling were simulated using the Finite element analysis (FEM) approach and are presented in Fig. 4. A very large strain generated a high-

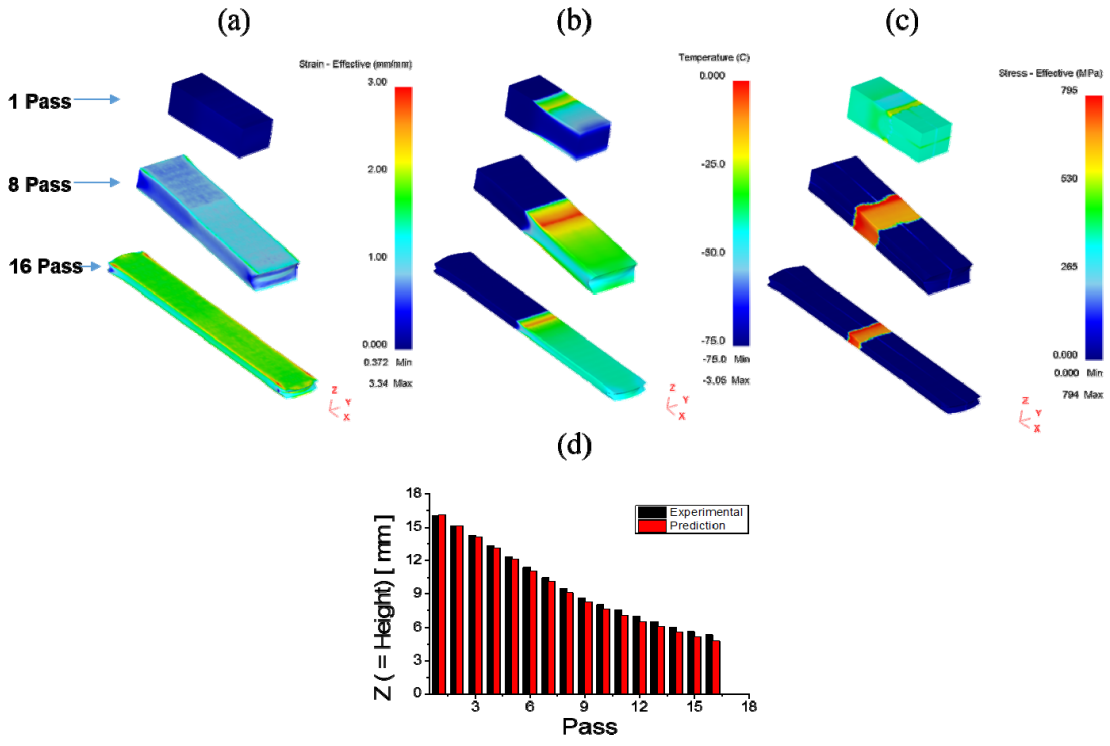

Fig. 4. (a) Strain during cryogenic rolling calculated by simulation, (b) stress, (c) temperature, and (d) sample height per each pass

stress level after 18 rolling passes. During the rolling process, the local temperature at the contact area with the roller experienced a significant increase owing to deformation heating, reaching up to –3°C. However, the average temperature was successfully maintained below –30°C after passing through the roll die. By ensuring sufficient cooling time between each pass, the plate temperature was set to –75°C for each pass. The experimental measurements of the heights closely matched the simulated heights (as shown in Fig. 4d), demonstrating the reliability of the FEM simulation results.

The grain-size evolution during the rolling and subsequent annealing processes was closely related to the accumulated strain and temperature, which varied with the position of the plate. A microstructure prediction module pre-implemented in the DEFORM-3D FE code was utilized to predict the microstructural variations during cryogenic rolling. A flowchart of the microstructure-prediction module implemented in the FE code is shown in Fig. 5(a). The grain-growth exponent (n) and activation energy (Q_g) for grain growth were 2 and 100 kJ/mol, respectively. Fig. 5b shows the FEM predictions for the aver-

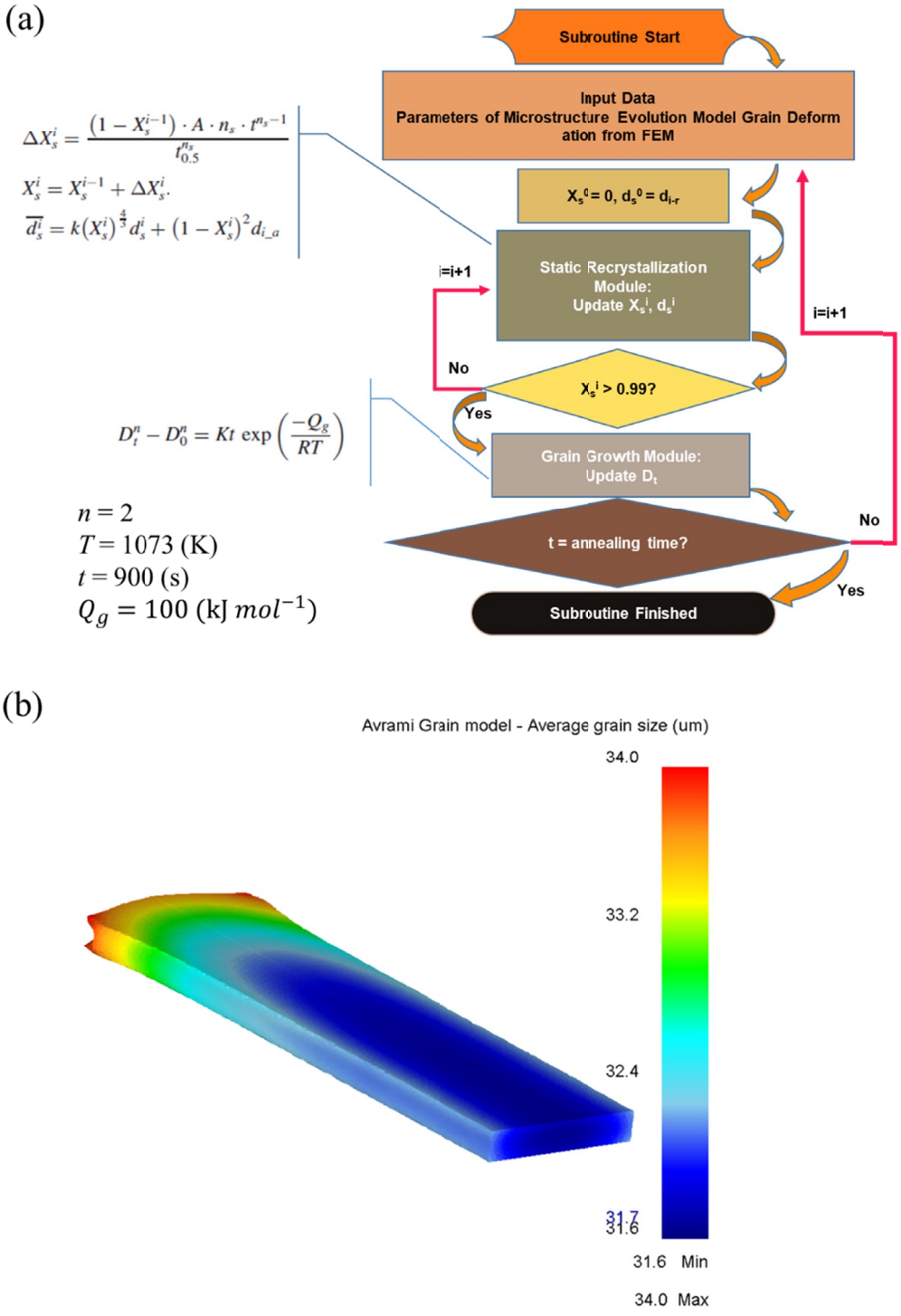

Fig. 5. (a) Flow chart of a microstructure prediction module for the recrystallization and grain growth models. (b) Distribution of FEM-predicted average grain size for the CT sample after annealing

age grain size of the CT sample after annealing at 800°C for 5 min. The grain size at the tail edge region was larger than that in the inner region because of faster thermal diffusion. Generally, the simulation results were in excellent agreement with the experimental observations, although some inconsistencies were observed. These inconsistencies may be attributed to the deviation between the actual and simulated temperatures.

4. Conclusions

In this study, we confirmed that cryogenic rolling can effectively refine the grain size of pure titanium produced by electron beam melting. The average grain size of pure titanium rolled with a reduction ratio of 70% in a –75°C atmosphere and subjected to annealing was found to be 29 μm. Furthermore, the (0001) basal texture of the cryogenically rolled sample exhibited improved alignment along the ND compared to the sample rolled at RT. The stress, strain, and temperature changes during rolling were simulated using an FE code, and reasonable predictions of the grain size evolution were obtained for the CT samples.

Acknowledgments

This work was supported by the Technology Innovation Program (grant number 20010047, "Development of deoxidation refining process using off grade Ti scrap over 100 kg per day for the production of 4N5 grade ingot and utilizing powder technology") funded by the Ministry of Trade, Industry & Energy, Korea). This study was supported by the Fundamental Research Program of the Korea Institute of Material Science (Grant number PNK8180).

REFERENCES

[1] Y.L. Zhou, M. Niinomi, T. Akahori, M. Nakai, H. Fukui, Comparison of various properties between titanium-tantalum alloy and pure titanium for biomedical applications. Materials Transactions **48**, 380-384 (2007).
DOI: https://doi.org/10.2320/matertrans.48.380

[2] D. Banerjee, J. Williams, Perspectives on titanium science and technology. Acta Materialia **61**, 844-879 (2013).

[3] E. Marin, M. Pressacco, S. Fusi, A. Lanzutti, S. Turchet, L. Fedrizzi, Characterization of grade 2 commercially pure Trabecular Titanium structures. Materials Science and Engineering C **33**, 2648-2656 (2013).
DOI: https://doi.org/10.1016/j.msec.2013.02.034

[4] C.W. Park, J.W. Park, K.C. Jung, S.-H. Lee, S.-H. Kim, J.H. Kim, Joint Properties of Inconel 718 Additive Manufactured on Ti-6Al-4V by FGM method. J. Korean Powder Metall. Inst. **28**, 417-422 (2021).
DOI: https://doi.org/10.4150/KPMI.2021.28.5.417

[5] M.A. Lodes, R. Guschlbauer, C. Körner, Process development for the manufacturing of 99.94% pure copper via selective electron beam melting. Materials Letters **143**, 298-301 (2015).
DOI: https://doi.org/10.1016/j.matlet.2014.12.105

[6] R. Guschlbauer, S. Momeni, F. Osmanlic, C. Körner, Process development of 99.95% pure copper processed via selective electron beam melting and its mechanical and physical properties. Materials Characterization **143**, 163-170 (2018).
DOI: https://doi.org/10.1016/j.matchar.2018.04.009

[7] J. Otubo, O.D. Rigo, C.M. Neto, P.R. Mei, The effects of vacuum induction melting and electron beam melting techniques on the purity of NiTi shape memory alloys. Materials Science and Engineering A **438-440**, 679-682 (2006).
DOI: https://doi.org/10.1016/j.msea.2006.02.171

[8] K. Yamanaka, W. Saito, M. Mori, H. Matsumoto, S. Sato, A. Chiba, Abnormal grain growth in commercially pure titanium during additive manufacturing with electron beam melting. Materialia **6**, 100281 (2019). DOI: https://doi.org/10.1016/j.mtla.2019.100281

[9] D. Gu, Y.C. Hagedorn, W. Meiners, G. Meng, R.J.S. Batista, K. Wissenbach, R. Poprawe, Densification behavior, microstructure evolution, and wear performance of selective laser melting processed commercially pure titanium. Acta Materialia **60**, 3849-3860 (2012).
DOI: https://doi.org/10.1016/j.actamat.2012.04.006

[10] H. Attar, M. Calin, L.C. Zhang, S. Scudino, J. Eckert, Manufacture by selective laser melting and mechanical behavior of commercially pure titanium. Materials Science and Engineering A **593**, 170-177 (2014).
DOI: https://doi.org/10.1016/j.msea.2013.11.038

[11] K. Yamanaka, W. Saito, M. Mori, H. Matsumoto, A. Chiba, Preparation of weak-textured commercially pure titanium by electron beam melting. Additive Manufacturing **8**, 105-109 (2015).
DOI: https://doi.org/10.1016/j.addma.2015.09.007

[12] J.-M. Oh, J. Yang, J. Yoon, J.-W. Lim, Effective Method for Preparing Low-Oxygen Titanium Ingot by Combined Powder Deoxidation and Vacuum Arc Melting Processes. Korean J. Met. Mater. **59**, 149-154 (2021).
DOI: https://doi.org/10.3365/KJMM.2021.59.3.149

[13] M. Vopsaroiu, M.J. Thwaites, S. Rand, P.J. Grundy, K. O'Grady, Novel sputtering technology for grain-size control. IEEE Transactions on Magnetics **40**, 4, 2443-2445 (2004).
DOI: https://doi.org/10.1109/TMAG.2004.828971

[14] S. Jurac, R.E. Johnson, B. Donn, Monte Carlo Calculations of the Sputtering of Grains: Enhanced Sputtering of Small Grains. The Astrophysical Journal **503**, 247-252 (1998).
DOI: https://doi.org/10.1086/305994

[15] M. Kumar, S.A. Khan, F. Singh, A. Tripathi, D.K. Avasthi, A.C. Pandey, Influence of grain size on electronic sputtering of LiF thin films, Nuclear Instruments and Methods in Physics Research. Section B: Beam Interactions with Materials and Atoms **256**, 328-332 (2007). DOI: https://doi.org/10.1016/j.nimb.2006.12.021

[16] T. Akatsu, C. Scheu, T. Wagner, T. Gemming, N. Hosoda, T. Suga, M. Rühle, Morphology and microstructure of the Ar+-ion sputtered (0001) α-Al2O3 surface. Applied Surface Science **165**, 159-165 (2000). DOI: https://doi.org/10.1016/S0169-4332(00)00376-7

[17] W.A. Abdallah, A.E. Nelson, Characterization of MoSe2(0001) and ion-sputtered MoSe 2 by XPS. Journal of Materials Science **40**, 2679-2681 (2005).
DOI: https://doi.org/10.1007/s10853-005-2104-7

[18] S.F. Chichibu, T. Yoshida, T. Onuma, H. Nakanishi, Helicon-wave-excited-plasma sputtering epitaxy of ZnO on sapphire (0001) substrates. Journal of Applied Physics **91**, 874-877 (2002).
DOI: https://doi.org/10.1063/1.1426238

[19] G. Sun, J. Xu, P. Harrowell, The mechanism of the ultrafast crystal growth of pure metals from their melts. Nature Materials **17**, 881-886 (2018).
DOI: https://doi.org/10.1038/s41563-018-0174-6

[20] E.A. Holm, S.M. Foiles, How grain growth stops: A mechanism for grain-growth stagnation in pure materials. Science **328**, 1138-1141 (2010).
DOI: https://doi.org/10.1126/science.1187833

[21] N. Bozzolo, N. Dewobroto, T. Grosdidier, F. Wagner, Texture evolution during grain growth in recrystallized commercially pure titanium. Materials Science and Engineering A. **397**, 346-355 (2005). DOI: https://doi.org/10.1016/j.msea.2005.02.049

[22] Y. Wang, T. Jiao, E. Ma, Dynamic Processes for Nanostructure Development in Cu after Severe Cryogenic Rolling Deformation. Materials Transactions **44**, 1926-1934 (2003).
DOI: https://doi.org/10.2320/matertrans.44.1926

[23] S. Jin, H. Liu, R. Wu, F. Zhong, L. Hou, J. Zhang, Combination effects of Yb addition and cryogenic-rolling on microstructure and mechanical properties of LA141 alloy. Materials Science and Engineering A **788**, 139611 (2020).
DOI: https://doi.org/10.1016/j.msea.2020.139611

[24] W. Cheng, W. Liu, S. Yuan, Deformation behavior of Al–Cu–Mn alloy sheets under biaxial stress at cryogenic temperatures. Materials Science and Engineering A **759**, 357-367 (2019).
DOI: https://doi.org/10.1016/j.msea.2019.05.047

[25] G. Shin, Y. Park, D.W. Kim, J.H. Yoon, J.H. Kim, Effect of Post-Weld Heat Treatment on Microstructure and Hardness Evolution of Functionally Graded Materials Produced by Direct Energy Deposition. Korean J. Met. Mater. **59**, 81-98 (2021).
DOI: https://doi.org/10.3365/KJMM.2021.59.2.81

[26] T.J. Collins, ImageJ for microscopy. BioTechniques **43**, S25-S30 (2007). DOI: https://doi.org/10.2144/000112517

[27] C.A. Schneider, W.S. Rasband, K.W. Eliceiri, NIH Image to ImageJ: 25 years of image analysis. Nat Methods **9**, 671-675 (2012).
DOI: https://doi.org/10.1038/nmeth.2089

[28] J.O. Obiko, F.M. Mwema, M.O. Bodunrin, Finite element simulation of X20CrMoV121 steel billet forging process using the Deform 3D software. SN Appl. Sci. **1**, 1044 (2019).
DOI: https://doi.org/10.1007/s42452-019-1087-y

[29] Abdulkadir Yıldız, Abdullah Kurt, Selçuk Yağmur, Finite element simulation of drilling operation and theoretical analysis of drill stresses with the deform-3D. Simulation Modelling Practice and Theory **104**, 102153 (2020).
DOI: https://doi.org/10.1016/j.simpat.2020.102153